Supporting Information for

A Cooperative Reformable Channel System with Unique Recognition of Gas Molecules in a Zeolitic Imidazolate Framework with Multi-Level Flexible Ligands

Benyamin Motevalli,[§] Huanting Wang,[†] and Jefferson Zhe Liu[§,*]

[§]Department of Mechanical and Aerospace Engineering, Monash University, Clayton, Victoria 3800, Australia

[†]Department of Chemical Engineering, Monash University, Clayton, Victoria 3800, Australia

Table S1. Summary of the permeance and separation performances of ZIF-8 and ZIF-L membranes for H_2, N_2, and CO_2 in experiments.

Figure S1. Crystal structures of the main cage of ZIF-L. Two methyl heads point toward the centre of the cage, leading to a significantly constrained void dimension at the centre.

Figure S2. Deformation of the *b*- gate of ZIF-L caused by a gas molecule (a) CO_2 or (b) N_2 at the gate centre.

Figure S3. Structure and charge analysis of the guest-host complex at *b*- gate. (a) Interatomic distances for CO_2 at the centre of *b*-gate. (b) Interatomic distances for N_2 at the centre of *b*-gate.

Figure S4. A cartoon to demonstrate the crowded and narrow channel passing through the 6-membered ring window (side view) in *c*- crystal direction of ZIF-L. A curvy diffusion path is depicted. The presence of two FLs enforces the orientation of the CO_2 molecule to be parallel to the 6MR plane.

Figure S5. A charge difference analysis when (a) CO_2 or (b) N_2 molecule passes through the 6-MR window in the channel along *c*- crystal direction.

Table S1 A summary of the permeability and selectivity of ZIF-8 membranes for H_2, N_2, and CO_2 gases measured in experiments. The results of ZIF-L membranes from this work are shown for comparison. Overall the permeability of ZIF-8 membranes for different gases follows the sequence $H_2 > CO_2 > N_2$. This is consistent with the kinetic diameter of the gas molecules, H_2 (2.9 Å), CO_2 (3.3 Å), and N_2 (3.64 Å). Considering that ZIF-8 does not have a continuous channel system, the molecular gating mechanism is a plausible explanation for the experimental observation. Interestingly, our ZIF-L membrane has a much better permeability for N_2 than CO_2, despite that N_2 has a larger kinetic diameter than CO_2. The ideal selectivity of ZIF-8 and ZIF-L membranes was calculated and is shown in Table S1. We also carried out gas separation experiments for gas mixture to determine the selectivity for H_2/CO_2 and H_2/N_2.

Table S1. Summary of H_2, N_2, and CO_2 permeance and separation performance of ZIF-8 and ZIF-L membranes in experiments.

				Permeability (10^{-2} mol·m^{-3}·s^{-1}·Pa^{-1})			Thickness		
Membranes	H_2/N_2	H_2/CO_2	CO_2/N_2	H_2	N_2	CO_2	(μm)	Condition	Ref*
ZIF-8	11.5	4.5	2.6	0.020	0.002	0.004	30	Ideal	1
ZIF-8	12.0	5.2	2.3	0.096	0.008	0.018	25	Ideal	2
ZIF-8	4.0	2.8	1.4	1.440	0.360	0.520	2.5	Ideal	3
ZIF-8	7.3	5.2	1.4	2.200	0.302	0.424	5	Ideal	4
ZIF-8	11.0	3.9	2.9	7.700	0.700	2.000	2	Ideal	5
ZIF-8	10.0	4.6	2.2	0.190	0.019	0.041	1	Ideal	6
ZIF-8	12.3	3.5	3.5	0.358	0.029	0.102	12	Ideal	7
ZIF-8	11.7	3.7	3.1	0.088	0.008	0.024	20	Ideal	8
ZIF-8	9.2	5.4	1.7	0.730	0.079	0.135	10	Ideal	9
ZIF-8	10.4	4.1	2.6	0.260	0.025	0.064	8	Ideal	10
ZIF-L	3.9	5.5	0.70	4.200	1.080	0.760	10	Ideal; b-oriented	11
ZIF-L	5.7	10.4	0.54	16.920	2.980	1.620	5	Ideal; c-oriented	11
ZIF-L	3.8	5.3	0.73	1.690	0.440	0.320	10	Ideal; b-oriented; PFA treatment	11
ZIF-L	8.1	24.3	0.33	3.900	0.480	0.160	5	Ideal; c-oriented; PFA treatment	11
ZIF-L	3.8	4.9						Binary; b-oriented; PFA treatment	11
ZIF-L	7.7	15.2						Binary; c-oriented; PFA treatment	11

* Reference 1 to 10 correspond to reference 22 to 31 in main text. Reference 11 corresponds to reference 21 in main text.

Figure S1 shows the zoom-in view of crystal structures of the main cage. The blue iso-surface shows the size and shape of the main cage. As seen, there are two methyl heads (dashed box) pointing to the centre of the cage, hence narrowing the cage at this cross-section. As a result, a small peak is observed in the energy profiles of N_2 and CO_2 at the centre, indicating that these gases experience a repulsive interaction from the methyl heads. This helps understand why the most favourable adsorption site of CO_2 or N_2 is not in the exact centre of the main cage of ZIF-L (Figure 2).

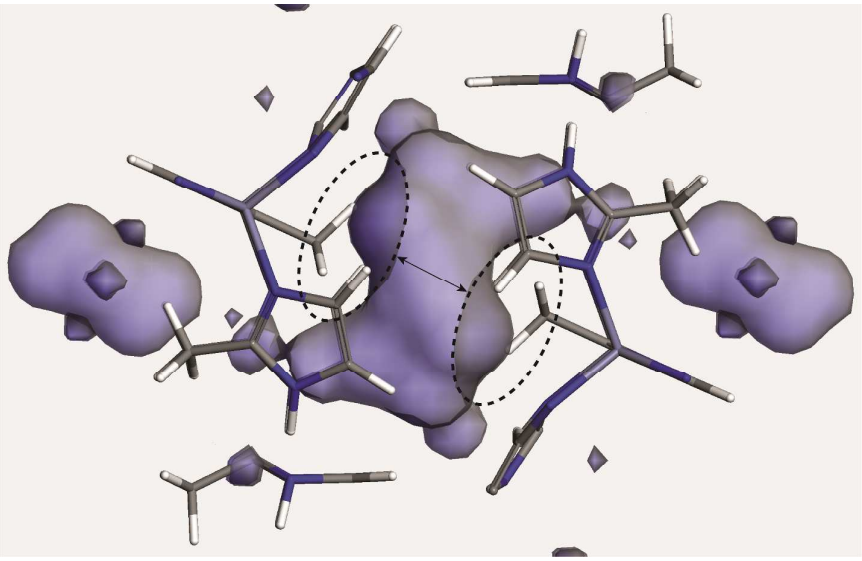

Figure S1. Crystal structures of the main cage of ZIF-L. Two methyl heads point toward the centre of the cage, leading to a significantly constrained void dimension at the centre.

ZIF-L does not have a continuous channel system (Figure 2). Those molecular gates that block the channels must be opened to allow the passage of gas molecules. The traditional view of such a molecular gating effect believes the 'size' of the gas molecules play a decisive role in determining the channel deformation (or gating opening) and thus dictate the permeance of the membranes for different gases. It is generally accepted that CO_2 has a smaller cross-sectional diameter than N_2, *i.e.*, 3.3 vs. 3.64 Å. Thus it is reasonable that CO_2 deforms the gates/channels less significantly than N_2. DFT calculations were carried out to confirm this expectation in our ZIF-L crystal. Figure S2 (a) and (b) show the deformation of *b*-gate in ZIF-L. Indeed, N_2 has led to a more

significant deformation. Consequently, N_2 should have a higher energy barrier for its transport in ZIF-L, and thus a lower permeability. But this is in contrast to the experimental results. We can conclude that the gate opening mechanism cannot explain the interesting permeability of ZIF-L membranes.

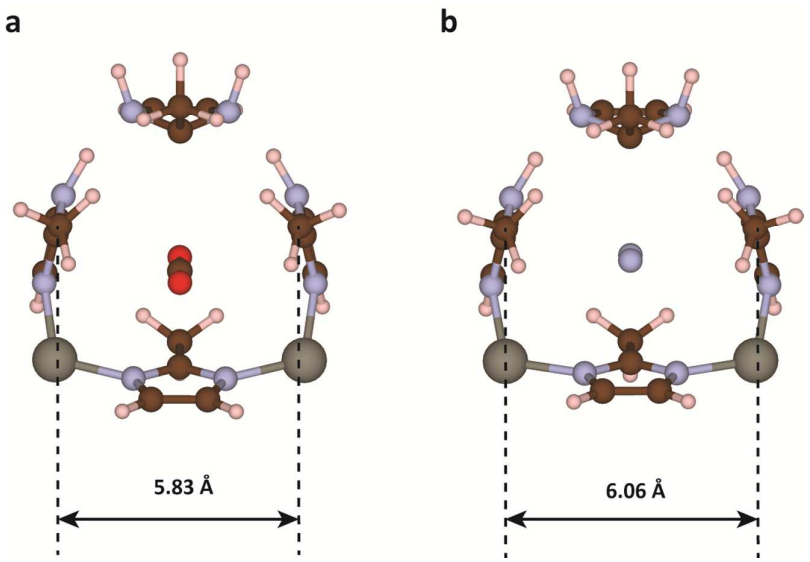

Figure S2. Deformation of the *b*-gate of ZIF-L caused by a gas molecule (a) CO_2 or (b) N_2 at the gate centre.

To understand why the N_2 has a less positive binding energy (i.e., less 'repulsive' interaction) at the *b*-gate centre despite it deforms the gate more significant than CO_2 molecule, we examined the chemical interactions between the gas molecules and gating molecules (one CL, two TLs, and one FL). The charge difference analyses and Bader analysis shown in Figure 4(a)-(d) indicate stronger charge redistribution for the case of N_2. For the case of CO_2, it can be noticed that the atomic charge changes mainly occurs on O_1 atom (on CO_2 molecule), the connecting ligand (C_3 and C_4), and the hydrogen atoms of the two methyl-heads. Overall the N_2 case has a more significant atomic charge change. It mainly happens on the N_2 molecule, the FL ligand, and the CL. Another evidence to demonstrate the stronger interaction of N_2 to the *b*- gate is the interatomic distance. The shortest distance between N_2 and the FL is only about 2.54 Å, much shorter than that of CO_2, 3.04 Å as seen in Fig. S3.

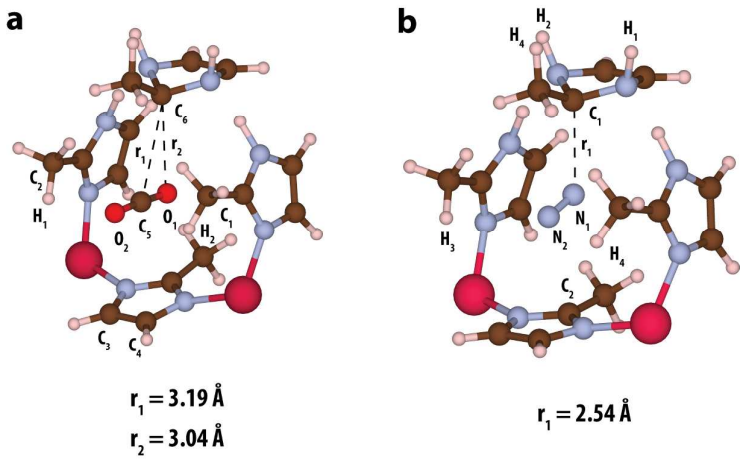

Figure S3. Structure and charge analysis of the guest-host complex at *b*- gate. (a) the Bader analysis and (b) Interatomic distances for CO_2 at the centre of *b*-gate. (c) The Bader analysis and (d) interatomic distance for N_2 at the centre of *b*-gate.

Figure S4 depicts the diffusion path of a CO_2 molecule through the 6MR window along the *c*- channel. It is seen that the 6MR gateway (side view) is blocked from both sides by the two FLs. Some critical interatomic distances are shown. For example, the two FLs are distanced about 2.78 Å, making this cross-section too compact. Such a compact configuration enforces the gas molecule to re-orient when passing through the 6MR gate, so that the longer dimension of the gas molecule would be parallel to the 6MR plane. Hence, instead of the kinetic cross-section diameter, the longer dimension of the gas molecules plays the major rule in selective recognition.

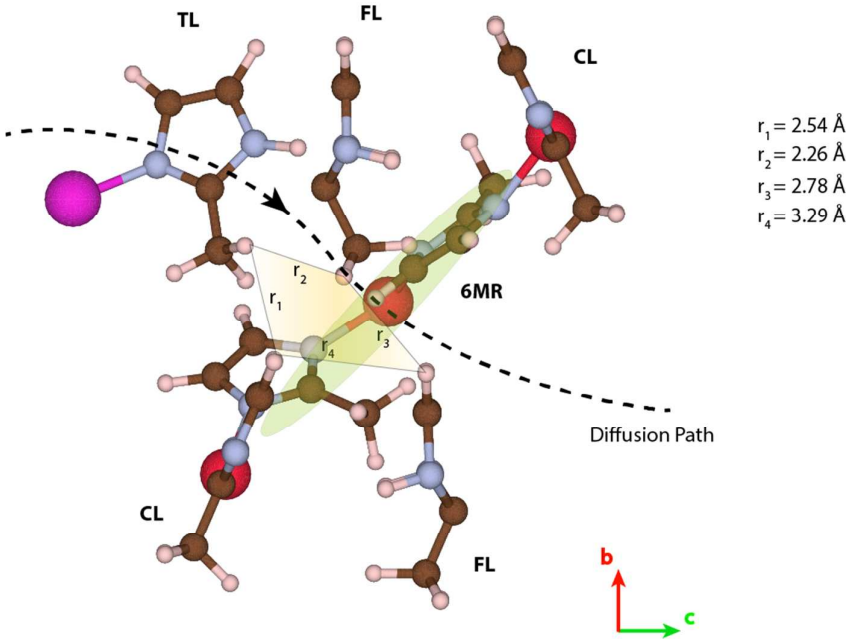

Figure S4. A cartoon to demonstrate the crowded and narrow channel passing through the 6-membered ring window (side view) in *c*- crystal direction of ZIF-L. A curvy diffusion path is depicted. The presence of two FLs enforces the orientation of the CO_2 molecule to be parallel to the 6MR plane.

Figure S5 shows the charge difference analysis for the guest-host complex when CO_2 or N_2 is passing through the 6MR gateway. This configuration corresponds to the saddle point of the binding profile along the *c*- channel (Figure 2), where the gases experience the highest (positive) binding energy. Note that the gas molecules adaptively re-orient themselves to fit-in the flexible channel that has been deformed under the influence of the gas molecules. The charge difference analysis shows the charge re-distribution for these two cases are comparable, suggesting that the chemical interaction may not be the reason for the less positive binding energy of N_2 at the saddle point, which is in contrast with the case of *b*- gate.

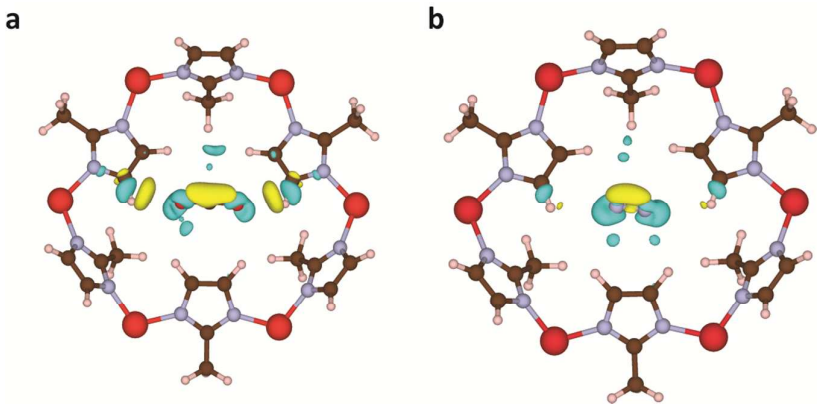

Figure S5. A charge difference analysis when (a) CO_2 or (b) N_2 molecule passes through the 6-MR window in the channel along *c*- crystal direction.

References

(1) Bux, H.; Liang, F. Y.; Li, Y. S.; Cravillon, J.; Wiebcke, M.; Caro, J. Zeolitic Imidazolate Framework Membrane with Molecular Sieving Properties by Microwave-Assisted Solvothermal Synthesis. J. Am. Chem. Soc. 2009, 131, 16000-16001.

(2) Shah, M.; Kwon, H. T.; Tran, V.; Sachdeva, S.; Jeong, H. K. One Step in situ Synthesis of Supported Zeolitic Imidazolate Framework ZIF-8 Membranes: Role of Sodium Formate. Microporous Mesoporous Mat. 2013, 165, 63-69.

(3) Pan, Y. C.; Lai, Z. P. Sharp Separation of C2/C3 Hydrocarbon Mixtures by Zeolitic Imidazolate Framework-8 (ZIF-8) Membranes Synthesized in Aqueous Solutions. Chem. Commun. 2011, 47, 10275-10277.

(4) Tao, K.; Kong, C. L.; Chen, L. High Performance ZIF-8 Molecular Sieve Membrane on Hollow Ceramic Fiber via Crystallizing-Rubbing Seed Deposition. Chem. Eng. J. 2013, 220, 1-5.

(5) Pan, Y. C.; Wang, B.; Lai, Z. P. Synthesis of Ceramic Hollow Fiber Supported Zeolitic Imidazolate Framework-8 (ZIF-8) Membranes with High Hydrogen Permeability. J. Membr. Sci. 2012, 421, 292-298.

(6) Shekhah, O.; Swaidan, R.; Belmabkhout, Y.; du Plessis, M.; Jacobs, T.; Barbour, L. J.; Pinnau, I.; Eddaoudi, M. The Liquid Phase Epitaxy Approach for the Successful Construction of Ultra-Thin and Defect-Free ZIF-8 Membranes: Pure and Mixed Gas Transport Study. Chem. Commun. 2014, 50, 2089-2092.

(7) Huang, K.; Dong, Z. Y.; Li, Q. Q.; Jin, W. Q. Growth of a ZIF-8 Membrane on the Inner-Surface of a Ceramic Hollow Fiber via Cycling Precursors. Chem. Commun. 2013, 49, 10326-10328.

(8) McCarthy, M. C.; Varela-Guerrero, V.; Barnett, G. V.; Jeong, H. K. Synthesis of Zeolitic Imidazolate Framework Films and Membranes with Controlled Microstructures. Langmuir 2010, 26, 14636-14641.

(9) Tao, K.; Cao, L. J.; Lin, Y. C.; Kong, C. L; Chen, L. A Hollow Ceramic Fiber Supported ZIF-8 Membrane with Enhanced Gas Separation Performance Prepared by Hot Dip-Coating Seeding. J. Mater. Chem. A, 2013, 1, 13046-13049.

(10) Zhang, X. F.; Liu, Y. G.; Kong, L. Y.; Liu, H. O.; Qiu, J. S.; Han, W.; Weng, L. T.; Yeung, K. L.; Zhu, W. D. A Simple and Scalable Method for Preparing Low-Defect ZIF-8 Tubular Membranes. J. Mater. Chem. A 2013, 1, 10635-10638.

(11) Zhong, Z.; Yao, J.; Chen, R.; Low, Z.; He, M.; Liu, J.Z.; Wang, H., Oriented Two-dimensional Zeolitic Imidazolate Framework-L Membranes and their Gas Permeation Properties. J. Mat. Chem. A (DOI: 10.1039/C5TA03707G, in press)